Amato, G., Eisank, C., Castro-Camilo, D. and Lombardo, L. (2019) Accounting for covariate distributions in slope-unit-based landslide susceptibility models. A case study in the alpine environment. Engineering Geology, 260, 105237.
(doi: 10.1016/j.enggeo.2019.105237)

There may be differences between this version and the published version. You are advised to consult the publisher's version if you wish to cite from it.

http://eprints.gla.ac.uk/195444/

Deposited on: 20 September 2019

Enlighten – Research publications by members of the University of Glasgow
http://eprints.gla.ac.uk

Accounting for covariate distributions in Slope-Unit-based landslide susceptibility models. A case study in the Alpine environment.

Gabriele Amato[1], Clemens Eisank[2], Daniela Castro-Camilo[3], Luigi Lombardo[4*]

September 20, 2019

Abstract

Thousands or even million of pixels can be contained in a single Slope Unit. Hence, each covariate used in spatial predictive models is characterized by a distribution of values for each Slope Unit.

Here, we model the whole covariates' distribution within Slope Units for landslide susceptibility purposes. This is done by finely dissecting each covariate into quantiles and then modeling the susceptibility via a LASSO penalized Binary Logistic Regression. We choose a LASSO penalization because the common Stepwise procedure is not selective enough to shrink a large number of covariates to an interpretable subset (which we also demonstrate here). LASSO mostly selects 6 covariates out of 372 to explain the spatial distribution of shallow landslides in the Upper Badia valley, Italian Alps. This allows us to verify that the selection does not include any quantile close to the median hence, nor to the mean. The latter is the common representation of the covariates' distribution within Slope Units, which we also test and report in the supplements. Overall, we suggest to always investigate the whole distribution because the mean may not be the most informative nor the most performing way to generate Slope-Unit-based susceptibility models. In this general context, we generate our landslide inventory by combining semi-automated (OBIA) and manual mapping procedures. Our inventory, quantile covariates' representation and LASSO penalization produce excellent performances and interpretable relations between covariates and landslides.

Keywords: Binary Logistic Regression, Landslide Susceptibility, Slope Units, Least Absolute Shrinkage Selection Operator (LASSO), Stepwise Selection, OBIA

Corresponding Author: Luigi Lombardo*, Email: l.lombardo@utwente.nl

[1]IFAC CNR, Via Madonna del Piano, 10, 50019 Sesto Fiorentino, Florence, Italy

[2]GRID-IT GmbH, Technikerstraße 21a, 6020 Innsbruck, Austria

[3]School of Mathematics and Statistics, University of Glasgow, Glasgow, G12 8QQ, UK

[4]University of Twente, Faculty of Geo-Information Science and Earth Observation (ITC), PO Box 217, Enschede, AE 7500, Netherlands

1 Introduction

Mapping units are defined as partitions of landscape with analogous geologic and/or geomorphic properties that differ from their surroundings across definable boundaries (Hansen, 1984). They are used in geomorphology to subdivide an area into objects upon which the probability of future landslide occurrences is estimated (Schlögel *et al.*, 2018). In particular, the Slope Unit (SU, hereafter) is a morphological feature that subdivides the land surface into subcatchment halves (Carrara, 1988). This is conceptually achieved by maximising the internal homogeneity of slope and aspect within individual SUs and the heterogeneity across adjacent SUs (Alvioli *et al.*, 2018). Therefore, a SU offers an ideal representation of space for which a SU approximates the morphodynamic response of a slope to a landslide (Lombardo *et al.*, 2018a). This property has historically made SU the only robust alternative to the common pixel choice (Reichenbach *et al.*, 2018). The first example of landslide susceptibility maps based on a SU partition can be traced back to Carrara *et al.* (1991). Since then, the community has made significant progress on how to compute SUs and how to implement them in the framework of landslide susceptibility models. Regarding the computation, the subjectiveness of SU delineation and mapping has been long left behind, initially by using the inverse DEM method (e.g. Zhou *et al.*, 2015) and more recently thanks to the software *r.slopeunits* introduced by Alvioli *et al.* (2016). This software efficiently calculates SU by using a DEM and a set of parameters. However, regarding the implementation in landslide susceptibility models, some questions still require careful consideration. For instance, a single SU may contain thousands or even millions of pixels depending on the resolution of the covariate set; hence, each SU is characterized by a distribution of values for each of the considered covariates. However, the geomorphological community has almost unanimously represented the aforementioned distribution simply through the mean and standard deviation (e.g., Guzzetti *et al.*, 2006; Rossi *et al.*, 2010). Representing a distribution via the two main statistical moments is valid if we assume the distribution to be Gaussian, and even in that case, landslide occurrences may be better correlated with values belonging to the

right or left tails. Only one case is currently available where the relation between landslide occurrences and the covariate distribution for each SU is considered more in depth (Castro Camilo *et al.*, 2017). There, the authors represent the covariates for each SU through 19 quantiles $(0.05, 0.10, ..., 0.95)$. And hypothesize that, if the approach that the community has pursued is correct, then a strong variable selection method would have extracted the median out of the 19 quantiles, as a proxy for the mean. The same article presents a new variable selection procedure in the geomorphological literature. Historically, the only variable selection method used in geomorphology has been the Stepwise, being it forward, backward or both (see Yesilnacar and Topal, 2005; Mathew *et al.*, 2009; Lombardo *et al.*, 2014; Cama *et al.*, 2015). However, the statistical community has highlighted numerous deficiencies in stepwise selection for several decades (Copas and Long, 1991; Derksen and Keselman, 1992) and proposed several preferable methods. For instance, Elastic Net (Zou and Hastie, 2005) and Least Absolute Shrinkage and Selection Operator (LASSO, Tibshirani, 1996) are both powerful methods which do not suffer from the same inadequacies of the stepwise (for a detailed description, see Harrell Jr, 2015). LASSO is particularly appealing, for it was also designed to tackle multicollinearity issues in large Generalized Linear Models (GLM, hereafter). Binary Logistic Regression (BLR), the method mostly used in the geomorphological community (Budimir *et al.*, 2015; Pourghasemi and Rossi, 2016) belongs to a GLM and therefore coupling LASSO to BLR when considering large landslide datasets is a convenient approach (Schillaci *et al.*, 2019). In Castro Camilo *et al.* (2017), the authors modeled deep-seated landslides in Japan and the code they used to generate the susceptibility model can be found in the supplementary material. Therefore, in this work we used their code aiming at replicating a similar experiment but on fast and shallow landslides in the Upper Badia Valley (Italy), a sector of the Italian Alps.

The rationale is similar to the one considered in Castro Camilo *et al.* (2017) for here we modeled the whole covariates' distribution within SU by finely slicing it into quantiles (with a 5 percentile step). And, we assumed that, if for rapid shallow landslides the traditional

representation of the distribution into mean and variance is enough, than LASSO would select the median value. We also test the validity of this hypothesis by using LASSO on a dataset made by using the traditional mean representation (check the Supplementary material for comparison) and run a parallel Stepwise selection to show the differences with respect to LASSO (see Appendix A). In this methodological context, we nested other geoscientific questions related to the landslide mapping procedure and to the geomorphological Alpine context. Specifically, we generated the landslide inventory by semi-automatically mapping shallow landslides using Object-Based Image Analysis (OBIA, hereafter) on the basis of high-resolution multispectral Pleiades satellite images and digital terrain layers. OBIA is a discipline aiming to develop automated methods to partition remote sensing imagery into meaningful image-objects. This is achieved on the basis of large sets of attributes, including spectral, geometrical and spatial properties. In turn, OBIA generates new geographic information in a GIS-ready format which can be used to address a wide array of scientific issues (Hay and Castilla, 2008).

Several examples are already available where OBIA has been tested to provide landslide inventories in a semi-automated and objective manner (Rau *et al.*, 2011; Hölbling *et al.*, 2012; Casagli *et al.*, 2016). However, these inventories (as many other semi-automated ones) are rarely used for susceptibility purposes (Reichenbach *et al.*, 2018).

Our work further explores not only the ability to produce automated inventories but to include them in a single landslide susceptibility modeling pipeline in line with comments made by Fan *et al.* (2018) and Van Westen *et al.* (2008).

Herein, we present our study as follows: in Section 2, we introduce the physiographic context; in Section 3, we explain how we generate the landslide inventory, first using OBIA to automatically extract the landslide signatures from satellite images and then manually polishing the inventory; in Section 4, we briefly describe current modeling trends in landslide susceptibility, (both for pixel and Slope Units) to show the difference with the approach we pursue as detailed in Section 4.1 and Section 4.2; we then describe in Section 5 and discuss in

Section 6 our results, only to conclude in Section 7. Additionally, Appendix A summarizes differences between LASSO and Stepwise procedures. And, Supplements provide readers with illustrations where the whole LASSO-penalized-BLR modeling pipeline has been run on the basis of a traditional mean representation of covariates per SUs.

2 Geological and Geomorphological context

The 181 km^2 study area is located in South-Tyrol (Italy) and it belongs to the Eastern Dolomites of the Italian Alps (see Figure 1). It extends to the upper part of Badia Valley (also locally referred to as Gadertal), where the Rio Gadera river flows, and includes the northern sector of the Puez-Odle-Gardenaccia and Fanes-Sennes-Braies Dolomites groups. These groups correspond to the natural boundary of the area to the West and East, respectively whereas the study area is bounded by the villages of San Martino in Badia to the North and Badia to the South.

The geological setting is characterized by an Upper Permian sedimentary succession. This succession begins with the fluvial Gardena Sandstone Formation (Fm), which unconformably overlies the crystalline basement belonging to the South-alpine metamorphic complex (Bosellini *et al.*, 2003). These formations are upwardly followed by transitional shallow marine evaporites and carbonates belonging to Bellerophon Fm. And, they all crop out in the NW of the study area.

The Lower Triassic Werfen Fm unconformably overlies the Permian sequence and consists of a complex succession of shallow-water carbonate and terrigenous deposits (Bosellini *et al.*, 2003), which largely crops out at low altitude in the central part of the study area.

Hyaloclastites and volcano-clastic basinal sediments, probably belonging to the Wengen Fm (Middle Triassic), as well as pelagic, grey-brown, marls and marly limestones, pertaining to the San Cassiano Fm (Middle-to-upper Triassic), crop out in the east and the south within the Rio Gadera valley.

Dolomite and shallow-water calcareous lithologies, related to Sciliar, Dolomia Principale

and Calcari Grigi formations (Middle Triassic Lower Jurassic), are present at high altitude along the western and southern margins, in correspondence of the aforementioned Puez-Odle-Gardenaccia and Fanes-Sennes-Braies mountain groups.

Geomorphologically, these lithologies constitute the highest reliefs in the area and confer to the landscape the characteristic aspect of rocky vertical cliffs, typical of the Dolomites. Such reliefs are linked to gentle slopes made up of the softer pelagic clayey bedrock, which underlie slope debris deposits produced by rock avalanches and rock falls that frequently detach from the dolomite and calcareous cliffs.

Overally gravitational processes have been shaping the general landscape of the Badia Valley at least since the Last Glacial Maximum (Vandelli *et al.*, 2019) and more recently during the Holocene (Soldati *et al.*, 2004). In this context, shallow landslides, like debris flows, and deeper earth flows or rotational slides are largely documented in the area (Soldati *et al.*, 2004; Marchetti *et al.*, 2017; Schlögel *et al.*, 2017). Specifically in the study area, these types of landslide preferentially affect the clayey bedrock, such as San Cassiano Fm, as reported by the landslide inventory compiled in the framework of the IFFI project (Trigila *et al.*, 2007).

Furthermore, remnants of Late Glacial lateral moraines testify the glacial advances during the Upper Pleistocene. These moraines can be found in the southern sector and well preserved glacial cirques are present within the Gardenaccia group (Marchetti *et al.*, 2017).

No indications of current permafrost are reported by the Alpine Permafrost Index Map (APIM) below 2300 m.a.s.l. (Boeckli *et al.*, 2012). In particular, APIM infers the possible presence of permafrost at higher altitude, within the dolomite massif groups and in some cases only in correspondence of north facing slopes.

Ultimately, data recorded at various meteorological stations in the Upper Badia show that January is the coldest month (mean Temperature = $-5°$ to $-7°$). Conversely, July represents the warmest month (mean Temperature = $12°$ to $15°$). Overall, the yearly mean air temperature is approximately $2.5°$ to $4°$ depending on the elevation. The precipitation

regime reaches its maximum from May to August, while January is usually the driest month (Ghinoi and Chung, 2005).

3 Landslide Inventory via Object-Based Image Analysis

3.1 Data description

Shallow landslides often result as neo-formation phenomena and include different processes as debris flows, shallow earth slides and soil slips (Hutchinson, 1988; Hungr *et al.*, 2014). Their failure surface generally develops at the contact between the regolith and the bedrock, roughly parallel to the slope, and their evidence tends to disappear within a few months/years (Piacentini *et al.*, 2012).

Our landslide inventory primarily consists of shallow landslides and was derived from multispectral and DEM-derived morphometric properties. Multispectral data consisted of a Pleiades satellite image acquired on 11 July 2011, this been delivered in 5 bands format, including RGB, Near-Infrared (NIR) and a panchromatic band (PAN). The PAN band was used to enhance the original spatial resolution of RGB and NIR from $2m$ to $0.5m$. Subsequently, the enhanced image was orthorectified by using both the Rational Polynomial Coefficients (RPC) which were included in the image metadata, and nine ground control points collected on a $20cm$ orthophoto. The absolute geolocation accuracy of the orthorectified image was $0.31cm$. In parallel, a Digital Elevation Model (DEM) at $5m$ spatial resolution was used to derive morphometric properties. The DEM originated from airborne laserscanning data, acquired in 2010, and provided by the Regional Government of South Tyrol, Italy, under open data policy. On the basis of the DEM and the pre-processed Pleiades image, we derived four information layers that served as additional input for landslide mapping. We computed *Slope* and *Terrain Roughness Index* (TRI) (Riley *et al.*, 1999). Since landslides generally trigger in steep terrain, slope is a well-suited layer for landslide detection. Terrain roughness was selected under the assumption that the surface of landslide areas is

usually rougher than the surface of the surrounding area. From the pre-processed Pleiades image, two multispectral layers were computed, the Normalized Difference Vegetation Index (NDVI) and image brightness. NDVI is a widely used indicator for the presence or absence of vegetation. Image brightness quantifies the "whiteness" of a surface. Generally, shallow landslide areas are characterized by *i*) missing or low vegetation cover which is indicated by low values of NDVI, and in turn *ii*) high presence of bare soil which is indicated by high values of brightness.

3.2 Landslide Inventory via Object-Based Image Analysis (OBIA)

We developed an object-based approach for shallow landslide inventory mapping. The mapping process was implemented in the open-source software InterIMAGE 1.43 (Costa *et al.*, 2010; Hölbling *et al.*, 2017). Due to limitations in handling larger datasets, we had to implement a tile-based processing scheme. Therefore, the selected data were split into 126 non-overlapping tiles. The size of each tile was $1.2 \times 1.2\ km$. The landslide mapping workflow was designed top-down and consisted of four cycles of segmentation and threshold-based classification. In the OBIA framework such an iterative workflow has been referred to as class modeling (Tiede *et al.*, 2010). We applied a region-growing segmentation algorithm to the pre-processed Pleiades image (Baatz *et al.*, 2000). Region growing iteratively merges adjacent pixels with similar spectral values to pixel clusters, so-called segments. The merging is controlled by spatial and spectral thresholds which have to be set by the user. We decided to balance the spectral and shape impact by defining values of 0.5. The third parameter, size, which is dimensionless, was set to 400. We found these values produced segments which corresponded well to the size of the smallest landslide areas. For the first cycle, the whole image was segmented; for the other cycles, segmentation was limited to those image parts which have been classified as landslide candidates in the preceding step. In each case, the segmentation algorithm was parameterized with the values mentioned above. Segments were tested against a threshold to decide whether they were classified as landslides. These thresh-

olds were selected on the basis of *i*) an exploratory analysis of segment properties and *ii*) recommendations given in the literature (Martha *et al.*, 2010; Eisank *et al.*, 2014). Classified segments of one cycle were merged and passed as region-of-interest to the next cycle. The decision rule applied in the first cycle was the following: "if the NDVI of a segment is below the mean NDVI of the tile, the segment is labelled as landslide". As result, we obtained a rather conservative classification of landslides with many over-classified areas. During the other cycles this initial landslide classification was continuously refined, including the removal of over-classification. In the second cycle, the decision rule was based on a brightness threshold. Segments with brightness values below the tile average were removed from the extracted landslide candidates of the first cycle. Then, in the third cycle, a slope threshold of 30° was implemented. Only segments with higher slope values than the threshold remained classified as landslides. In the last cycle, a TRI threshold of 1.5 was used to decide if the classification of a segment as landslide was kept or removed. Segments with TRI values below the threshold were removed from the result of the third cycle. Each tile was processed separately with the designed workflow. The extracted landslide polygons per tile were merged. We implemented a rule indicating that if a polygon had been split at the tile border, the two parts of the polygon were combined in the merged inventory. Landslide polygons with an area below $100m^2$ were filtered from the inventory, since the spatial resolution of the DEM was too coarse for extracting landslides with spatial extents below $10m$. The final landslide inventory for the study area comprised 2763 polygons.

3.3 OBIA limitations and expert-based solutions

Despite the complex classification workflow, when looking at the resulted polygons, some spurious classifications still remained. The main source of misclassification consisted of Type I errors where landslides were mapped on purely carbonatic outcrops (see Figure 2). Unfortunately, a large proportion of landslide scars in the area often correspond to mass movements which mobilize the whole regolith and expose the bedrock underneath. OBIA recognized

this pattern and assigned a landslide presence even for cases where the bedrock naturally outcrops. To eliminate these False Positives, we manually revised the semi-automated inventory. The task was quite simple to accomplish for the Type I errors were all clustered on carbonatic lithologies, making the interpretation of available orthophotos and geological information a rapid criterion to filter out misclassifications.

The remaining inventory added up to 1939. However, OBIA combined into a single landslide body contributions originated from separate lobes which in reality only merged during the propagation phase. The main purpose of landslide susceptibility studies is to learn from location where the process initiated and derive functional relationship on a covariate set upon which making a prediction. As a result, we assumed that using a single landslide polygon instead of its multiple contributing lobes would have yield two primary issues in our model. The first issue could have consisted of a poorer dataset where the actual landscape properties leading to slope instability would have been masked out from the analyses. The other issue would have resulted from our representation of slope instability. In fact, we assumed the landslide source point to be the highest location along the landslide boundary and by using a single polygon, the actual source point may have been extracted at locations where no instability occurred. As a result, we opted to manually map the highest source point of each landslide lobe for those multiple landslide polygons that OBIA interpreted as one. Specifically, we did not map the source point of rockfall deposits, which likely are located within the bedrock exposure areas. However, we mapped the source points of shallow failures that initiated within the slope debris deposits produced by previous rock avalanches and falls. The final inventory consisted of 2282 detachment points that we used as reference data for the susceptibility model.

4 Statistical modeling

Spatial predictive models represent the primary tool for assessing landslide susceptibility at catchment or regional scales (Brenning, 2005), although the choice of the best mapping unit

is not always straightforward. The Pixel is the most common unit. However, several studies show that for flow-like landslides, the high resolution provided by using a fine squared lattice provides worst results compared with a coarser pixel (Cama *et al.*, 2016; Arnone *et al.*, 2016). Therefore, there are physical processes that require to be modeled as broader areal features rather than point features. Slope Units are one of these areal features and some studies report their performance to be similar or even better than their grid counterpart (Erener and Düzgün, 2012; Van Den Eeckhaut *et al.*, 2009). For this reason, we focus on Slope Units, trying to investigate one of the main modeling problems for such mapping unit namely, how to express the distribution of each covariate inside a Slope Unit. To do this, we follow the approach described by (Castro Camilo *et al.*, 2017) and sample each continuous covariate via 19 quantiles. However, such procedure makes the predictor hyperspace 19 times larger and induces strong multicollinearity in the data. To account for this, we use the LUDARA code attached to Castro Camilo *et al.* (2017) as explained in sections Section 4.1 and Section 4.2.

4.1 Covariates

The initial number of covariates we chose was 26. They consist of SU morphologic indices, distance to faults, to roads and to lithological contacts as well as DEM-derived moprhometric properties, NDVI and thematic information coming from the local geological, land use and soil maps. We used the $5m$ DEM, adopted for the landslide inventory, to compute the following derivatives: *Slope* (Zevenbergen and Thorne, 1987), *Eastness* and *Northness* (computed as the sine and cosine of the Aspect, respectively) (Lombardo *et al.*, 2018b), *Planar* and *Profile Curvatures* (Heerdegen and Beran, 1982), *Relative Slope Position* (RSP, Böhner and Selige, 2006), *Stream Power Index* (SPI, Moore *et al.*, 1991), *Topographic Roughness Index* (TRI, Riley *et al.*, 1999), *Topographic Positioning Index*, *Topographic Wetness Index* (TWI, Beven and Kirkby, 1979). Additionally, we also derived the *Temporal Mean of NDVI* and *Temporal Standard Deviation of NDVI* (Rouse Jr *et al.*, 1974) from Landsat 5 scenes

acquired on: 25^{th} of September 2003, 27^{th} of September 2004, 1^{st} of September 2006, 18^{th} of July 2007, 23^{rd} of July 2009 and 12^{th} of September 2010 (at a 30m resolution). The images were collected during summertime to avoid cloud coverage.

The same DEM was used to compute slope units via r.slopeunits (Alvioli *et al.*, 2016). From those, we computed the following morphometric indices: *i*) Maximum Distance; *ii*) Maximum Distance divided by SU area; *iii*) Maximum Distance divided by the square root of the SU area; *iv*) SU Perimeter divided by SU area; *v*) SU Perimeter divided by the square root of the SU area; *vi*) Shape Index (Forman and Godron, 1986).

The distance to faults was computed as the Euclidean distance between each pixel centroid and the nearest tectonic line. The resulting shapefile was rasterized to coincide with the DEM resolution. The same was done to compute the covariates *Distance to roads* and *Distance to lithological contacts*.

As regards the thematic properties, we opted to compute the ratio between each categorical class extent and the total surface of the SU intersecting it. As a result, the *Outcropping Lithology* was retrieved from the local Geological Map of Italy at 1:500.000 scale. This map was based on 1:100.000 and 1:50.000 national geological cartography or geological maps (Tacchia *et al.*, 2005). In our case, we converted it into 12 ratios, each one expressed in percentage. Similarly, we converted into 5 ratios the Soil information reported in the soil map compiled by the European Commission - Joint Research Centre (Finke and Montanarella, 2001). As for Land Use, the Corine Land Cover (Büttner, 2014) product of 2012 was converted into 9 ratios.

This is a convenient representation of the categorical properties within a given area when using SU or any other irregular polygonal feature. In fact, the only alternative available in the literature is to compute the most frequent class contained in a SU and assign that value to the whole polygon (e.g. Tian *et al.*, 2010). In case of large landslide bodies, this procedure is justifiable for the larger the failing mass the less it should be sensitive to smaller conditions within the slope. However, for shallow landslides, we believe that such procedure

would disregard the contextual presence of other lithological or soil types within the same slope unit, thus neglecting their contribution to the failure mechanism and in turn, to the predictive model. Specifically for shallow and fast landslides, there is no actual evidence nor reason to think that predominant classes across a given SU are the only factors contributing to the failure mechanism. Shallow landslide initiation can take place in very small areas only to become larger while entraining other material during their propagation phase.

4.2 Binary Logistic Regression and LASSO penalization

Binary Logistic Regression (BLR) is a probabilistic model used in landslide susceptibility to explain the distribution of landslides over space. This is commonly done by using a Generalized Linear Model (GLM) which is able to handle response variables of several linear exponential families. Specifically, in susceptibility studies, we assume the linear exponential Bernoulli distribution to be able to explain landslide occurrences when they are summarized in a dichotomous (*Landslide/No-Landslide*) data structure. A BLR model can be summarized as follows:

$$P = \frac{e^{\beta_0 + \sum_{j=1}^{J} \beta_j x_j}}{1 + e^{\beta_0 + \sum_{j=1}^{J} \beta_j x_j}} \tag{1}$$

where P is the probability of landslide occurrence, β_0 represents the model intercept, β_j is the vector of coefficients which is multiplied by the vector of covariates x_j. These covariate are assumed to behave linearly.

The previous equation can be conveniently transformed as follows:

$$\eta_i(P) = \log\left\{\frac{P_i}{1 - P_i}\right\} = \beta_0 + \sum_{j=1}^{n} \beta_{ji} x_{ji} \tag{2}$$

where η_i is the logit link function and the linear model is isolated to the right side.

To compute the probability of landslide occurrence at a i^{th} mapping unit we can take the inverse of the logit function in Equation 2 as follows:

$$p_i = \frac{1}{1 + e^{-\eta_i}} \tag{3}$$

Ultimately, the estimation of the parameters on the right side of Equation 2 is performed maximizing the likelihood function:

$$\ell(\beta_0, \beta_1, \ldots, \beta_j) = \sum_{i:y_i=1} \log\{\pi(\boldsymbol{x}_i)\} + \sum_{i:y_i=0} \log\{1 - \pi(\boldsymbol{x}_i)\} \tag{4}$$

where $\pi(\boldsymbol{x}_i)$ is the probability that the i^{th} observation corresponds to a landslide presence at the i^{th} pixel or slope-unit. And, x_i is the covariate value at the same landslide presence case.

This is a well established model in the literature; however it may suffer from several issues depending on the data used for the analyses. One of the main issues relates to the number of predictors used to construct the model. When the predictors hyperspace is large, the model may exhibit multicollinearity, overcomplexity and limited interpretability.

Solutions for these issues have been already proposed via Penalized Logistic Models. Among them, the Least Absolute Shrinkage and Selection Operator (LASSO) represents a valuable tool to address the aforementioned issues (Tibshirani, 1996), for it penalizes the number of covariates while trying to maintain the overall predictive power. Specifically, LASSO performs simultaneous variable selection and parameter estimation and it is also designed to deal with multicollinearity. For this reason, it is well suited to tackle landslide susceptibility studies, especially in the present research where the total number of covariates is 372 due to the quantile representation (19 quantiles, from 0.05 to 0.95) of the covariate distribution within a slope unit.

Overall, LASSO operates by penalizing the likelihood ℓ shown in Equation 4:

$$\ell^{\star} = \ell - \lambda H \tag{5}$$

where the penalization of ℓ is performed by adding an extra term H which controls how reasonable the parameter estimation is, and λ, which acts to balance likelihood and penalty. Specifically, this is achieved as follows:

$$H = \lambda \sum_{j=1}^{n} |\beta_j| \tag{6}$$

where λ is multiplied to the absolute value of the vector of coefficients (also known as the $L^1 Norm$), forcing the value of non-informative coefficients to be null. For a more extensive explanation on LASSO and how to compute λ, we refer to Lombardo and Mai (2018) for a more geoscientific readership and to Tibshirani (1996) for a more statistically-oriented audience.

In the context of the present paper, we used a LASSO penalized Binary Logistic Regression model, to shrink the number of covariates to the ones that explain the distribution of landslides the most efficiently, within the study area.

In doing this, we implemented a combination of the LUDARA code used in Castro Camilo *et al.* (2017) and the one used in Lombardo and Mai (2018), computing 500 bootstrapped replicates. Each replicate is built by selecting at random 75% of the observed landslide presence cases and balancing it with an equivalent number of absences. The balanced dataset is fitted to the corresponding covariate set using the LASSO-BLR procedure explained above. For each fitting procedure, we perform a 500-fold cross-validation on the complementary 25% presence subset combined to an equal number of absences. Coefficient estimates, their LASSO penalization, and several performance metrics are stored at each iteration.

Specifically, we summarized the results as follows: *i*) Receiver Operating Characteristic curves (ROC), *ii*) their Area Under the Curve (AUC), *iii*) Accuracy ($(True\ Positives + True\ Negatives)/Total\ Sample$), *iv*) Error Rate ($mean(False\ Positives|False\ Negatives)$). The overall variability of these parameters is assessed across the 500 models. We also pro-

duced Error Plot (Mean Susceptibility VS Standard Deviation of the Susceptibility per SU), and a summary of the regression coefficients' distribution estimated over the 500 replicates.

5 Results

Any susceptibility model should undergo a performance evaluation phase, followed by an assessment of the coefficients' reasonability in a geomorphological sense. And, this should be completed by a graphical translation of the estimated probabilities into susceptibility map, together with their associated variability across replicates. In the present paragraph, we present the results according to this rationale.

Performance-wise, 500 ROC curves are shown in Figure 3a. Their mean AUC is 0.87 with an associated standard deviation of 0.02. This is already a good indicator of excellent performances according to Hosmer and Lemeshow (2000).

However, ROC curves do not provide information on the ability of any model to predict True Positives and Negatives as well as False Positives and Negatives. To take on this task, we measured the Accuracy, the model space between True Positives divided by Total Positives and True Negatives divided by Total Negatives, together with the error rate.

Figure 3b shows the Accuracy calculated for each replicate and for each probability cutoff between stable and unstable conditions. The average accuracy is 0.79 with associated variability measured with a standard deviation of 0.02. This indicates that, on average, the 500 susceptibility models predicted 79% of the Landslide and No-Landslide cases. Figure 3b is also particularly interesting because is shows the Accuracy as a function of the probability cutoff. Here, we reached the maximum Accuracy value along the dashed red line at a probability threshold equal to 0.46. This value is slightly lower than the usual 0.5 found in the literature (e.g. Frattini *et al.*, 2010; Süzen and Kaya, 2012; Raja *et al.*, 2017). In any other situation we should have adjusted all the calculation with a new probability cutoff, although for the present case, we left it at 0.5 for the difference in mean Accuracy between the two cutoffs is negligible.

An even better insight on the model behaviour when correctly predicting Landslide and No-Landslide conditions is provided in Figure 4. Here we show that on average, the model is more suited to predict No-Landslide conditions which are correctly predicted 80.1% of the times with an associated standard deviation of 3.24%. Conversely, 77.3% of Landslide-prone conditions are correctly predicted with a variability expressed in 2.8% within a single standard deviation.

Ultimately, the median of the error rate (ratio of failures' number to the number of the testing data points) is reported to be 0.215 with an inter-quartile distance of 0.029. This indicates that the model consistently and limitedly produces misclassified cases.

Assuming the performance to be consistently and reliably excellent, the other mandatory requirement is to assess whether the model estimates are reasonable from an interpretative standpoint. Figure 5 (left panel) shows the proportion of inclusion of all the covariates among the 500 replicates. Figure 5 (right panel) reports the same information but obtained from a Stepwise selection. Differences will be explained in Sections 6 and 7 as well as Appendix A, but the text below will only focus on LASSO. Six covariates are reported to be consistently selected above 80% of the bootstrapping procedure. These are *Rock outcrops/SU (%)*, *95% quantile of TWI*, *5% quantile of TWI*, *Sd of Elevation*, *Rendzic leptosol/SU (%)*, *Max SU length*, as shown in Figure 6. Here we plot the distribution of the coefficients' estimates, where the six respective median values are -0.53, -0.17, -0.24, 0.23, 0.06 and 0.09. It is important to remind that coefficients are all expressed in the same scale; thus, between covariates, the larger the difference in their absolute values the larger the influence to the final susceptibility.

Reporting regression coefficients is useful to recognize correlation patterns between covariates and landslides. However, for BLR is a multivariate model, looking at coefficients does not provide information on variable interactions and the resulting susceptibility estimates. To account for this, we plotted the average susceptibility (coming from the 500 replicates) against the original covariates in Figure 7. The rationale to read this plot is that

if a covariate had a predominant role in the model, then it's effect on the final probabilities should emerge or still be visible despite the contribution from the other additive terms. This is clear for continuous morphometric properties although for the categorical ratios it is less intuitive. Our interpretation will be provided in Section 6.

Ultimately, we extracted the probability estimates and converted them in map form. Figure 8 shows the mean susceptibility computed over the 500 replicates, together with the associated variability measured in one standard deviations (we do not plot it as a typical 2σ just to keep some spatial patterns visible for the reader). Because a multi-fold procedure returns several probability distributions over space (here 500), it is also useful to check which SU was consistently depicted as unstable. In other words, the SU where high susceptibility is associated to low variability represents the most hazardous locations. On the other hand, high susceptibility accompanied by high variance across replicates may lead to a lesser prioritization in remediation actions.

To summarize this information, we provide the error plot (Lombardo *et al.*, 2014, 2015) in Figure 9, where mean probabilities and their standards deviation are shown in a density scatterplot manner for clarity.

6 Discussions

The overall performance of our LASSO penalized BLR is excellent according to the classification proposed by Hosmer and Lemeshow (2000). To an average AUC of 0.87 calculated via a 500-fold CV procedure, we also added several complementary metrics to broaden the assessment on model hits and misses. This is summarized in Figures 3 and 4 where the robustness is highlighted by a very limited spread around the mean ROC and Accuracy curves, mean True Positive Rates VS True Negative Rates as well as the Error rates.

This is achieved by using few covariates thanks to the LASSO selection which successfully converges to an optimal solution 500 times out of 500 replicates (see Figure 5, left panel). Conversely, our Stepwise test fails for 71.2% of the 500 replicates, unable to handle a large

covariate set nor the multicollinearity which affects it.

LASSO consistently includes six covariates in the model (see Figure 5). These dominant properties are shown to contribute both negatively and positively to the susceptibility. Specifically, *Rock outcrops/SU (%)* contributes to indicate stable slope conditions and is also the covariate with the strongest influence. This is marked by a median regression coefficient equal to -0.53 (shown in Figure 6). Because we rescaled all the covariates prior to the anayses, the coefficients are expressed in the same scale. This makes it possible to objectively rank the covariate contributions by looking at the coefficients' absolute value. Its relevance to the model can also be seen in Figure 7 where the 0% values are clearly masked by other covariate interactions; however, where Rock outcrops cover the vast majority of the SU, then the corresponding susceptibility estimates are all confined below the 0.5 probability cutoff (marking stable conditions). A negative contribution of Rock outcrops to the susceptibility can be obviously interpreted in terms of absence of soil cover, a mandatory requirement to feed shallow landslide activations.

The second and fourth most influential covariates are *5% quantile of TWI* (median $\beta = -0.24$) and *95% quantile of TWI* (median $\beta = -0.17$). Here we skipped the third, because we believe it is important to draw attention to the coexistence of two TWI quantiles. Their presence should hint to multicollinearity and to the inability of LASSO to deal with such issue. However, we a posteriori checked the pairwise correlation between the two TWIs, finding a Pearson correlation coefficient of just 0.3. This is a value far from those reported to be diagnostic of existing collinearity (e.g. Dormann *et al.*, 2013). For this reason, we believe that LASSO may have picked up some non-linear signal brought by the TWI, which would have been lost by using the traditional mean value for SU. This is also visually supported in Figure 7 where the two TWI quantiles decrease the overall susceptibility but with slightly different patterns and in different ranges of TWI values. The TWI is a property which potentially indicates landscape morphology where overland water flows may accumulate. We recall here that TWI typically shows high values at valley floor, low values along the

watershed ridges and medium values within slopes. Hence, the greater the tendency for the water to accumulate (at valley floor) or to diverge (along the watershed), the lower the susceptibility. The module of the two TWI correlation coefficients may indicate a variation in the strength of the negative contribution, being stronger at lower TWI values. The third contributor to the model is the *Sd of Elevation* (with a median coefficient of 0.23). The standard deviation of the elevation within a SU can be seen as a proxy for different properties namely, slope steepness or more generally for topographic roughness. In the first case, low steepness angles have been empirically demonstrated to not be subjected to shallow landslides and in particular to debris flows (minimum angle equal to 15° in Costa, 1984; Iverson *et al.*, 1997; Imaizumi *et al.*, 2006). As regards the potential interpretation of topographic roughness, this is also a well-known parameter contributing to slope failures, especially in debris flow cases (Chen *et al.*, 2015; Tiranti *et al.*, 2018). Irrespective of the property the Sd of Elevation is mimicking in the model, Figure 7 shows how strong its influence is on the final susceptibility estimates. In a single-variable linear model, the relation between probabilities and covariate value should produce a straight line at 45°. Here, the densities still align in a straight line, and the contribution from the other covariates in the models is only shifting the trend towards the ordinate axis. The same thing cannot be said for the two TWIs where the linear trend gets masked by other contributions or multiple variable interactions.

An interesting property is shown to be the *Maximum SU length* (with a median coefficient of 0.09). This may indicate that the elongation of the SU may also play a role in the initiation process. Similarly to the consideration above, the SU elongation appears to retain some linearity in Figure 7, although in this case, other covariate influences produce a much larger spread (Carrara *et al.*, 2008).

Ultimately, *Rendzic leptosol/SU (%)* is reported to be the sixth contributor out of the six mostly selected covariates (with a median coefficient of 0.06). Its limited role in the model is confirmed even in Figure 7 where both 0% and 100% probability values are masked

by additional covariate terms. As reported in the World Reference Base for Soil Resources (Working Group WRB, 2014), Rendzic Leptosols typically develops from solid or unconsolidated rocky, highly calcareous material (limestone, dolomite, gypsum, and marlstone are among the most common primary rocks). It can be very shallow or deeper, but is usually extremely gravelly and/or stone-rich (Nachtergaele, 2010). Despite its low weight in the model, the occurrence of this type of soil can be interpreted as the natural consequence of the wide presence of calcareous bedrock in the study area. At the same time, this confirms the necessity of soil cover in order to favour shallow landslides.

Notably, LASSO selects a combination of morphometric, thematic and SU properties. These components could be translated into a simple conceptual model where morphometric covariates carry the broad topographic signal, whereas the SU length contributes with slope-specific information. This scheme is complemented by lithotechnical proxies able to approximate the mechanical behavior of the material involved in the failure mechanism (Lan *et al.*, 2004). Nevertheless, despite the high lithological variability in the study area (see Fig.1), no lithotypes have been selected as factors promoting landslide occurrences. A similar result has been obtained by (Castro Camilo *et al.*, 2017), where the authors modeled deep-seated landslides in Sado, Japan. There, LASSO selected sandstone as an indicator of stable conditions. And similarly to the present case, no other lithologies appeared to promote landsliding. One possible interpretation is that morphometric variables and SU characteristics can spatially carry some information coincident with lithotechnical parameters leading to landslide presence or even clustering effects (Lombardo *et al.*, 2019). Another explanation could be that soil type might be a much more informative covariate then bedrock lithology, especially for shallow landslides. In such cases, a substantial improvement could be achieved by accounting for the soil thickness when generating a susceptibility/hazard map (e.g., Bout *et al.*, 2018; Lombardo *et al.*, 2016).

Aside from covariates' effects, the final susceptibility map is shown in Figure 8. Here the north-eastern sector is shown to be much rougher and susceptible to shallow landslides.

In fact, SU are much smaller in this region compared to the west, which indicates that rapid changes in slope exposition occur, and in turn that a greater topographic variability characterizes the area. This also translates to susceptibility estimates. The north-eastern sector is very susceptible, with the exception of a clear non-susceptible linear pattern which belongs to a NW-SE oriented valley. This valley corresponds to a rupture of the slope gradient where debris material accumulates. Conversely, the south-eastern sector where the Dolomia Principale and the Calcari Grigi outcrop, shows the lowest susceptibility values. The rest of the map appears to be assigned with probabilities slightly higher than 0.5, taking aside the valley floors. A very beautiful example of two opposite facing slopes is shown in the central part of the study area, where two large SU stand out to be highly susceptible to debris flows.

A very limited spread characterizes the mean susceptibility as shown in the overall dark blue, standard deviation map in Figure 8. A better insight of this variability is shown in Figure 9. Here ideally the relationship between mean susceptibility and its standard deviation should depict a bell-shaped trend, with low variances assigned to the right and left tail of the mean probability distribution. And, acceptable higher variances, should appear in the central part of the plot where it is difficult to decide a perfect cutoff value between stable and unstable conditions. This ideal description is well represented in this Error plot, which suggests that where the model indicates high susceptibility, then this prediction is reliable at least over a random combination of 500 bootstrapped replicates within the area. Overall, we believe our workflow to be implementable both for landslide susceptibility and landslide hazard studies, both modeled via statistics and data mining approaches (Ko and Lo, 2018; Đurić *et al.*, 2019). Specifically, we suggest a similar approach in cases where the number of covariates is large and a reasonable subset is sought to simplify the engineering-geological interpretation of slope instability processes. In particular, our model relies on SUs with a mean extent of approximately $35000m^2$, which makes it a suitable scale also for site-specific engineering purposes (Lin *et al.*, 2018). In fact, the obtained susceptibility could be a reference for master planners to isolate potentially unstable slopes upon which further

investigate slope-specific hazard via deterministic approaches, especially for shallow and fast landslides (Lin and Lin, 2015; Horton *et al.*, 2019; Hu *et al.*, 2019).

Notably, in the Supplements we also provide the reader with further analyses aimed at replicating the workflow presented in the main manuscript, but using the traditional mean instead of the quantile-based dataset. The results show that: *i*) the performances are almost identical; *ii*) the variability estimated through the bootstrapped procedure is also analogous despite the initial larger degree of freedom of the quantile-model; *iii*) the susceptibility patterns do not change; iv) to reach the same level of performance the mean-based models require a greater model complexity, with 8/60 primary covariates instead of 6/372 (for the quantile one).

7 Conclusion

By modeling the whole covariates' distribution, we tested whether LASSO would have extracted median properties as a proxy for their mean value counterpart, which is generally used in SU-based susceptibility studies. Out of the six mostly selected covariates, none of them was close to the mean, which suggests that a better information could be obtained by modeling the entirety of the distribution rather than summarizing it into its main statistical moment. Despite we have run the same analyses for a mean-based traditional dataset (see the supplements) and found little differences with respect to the quantile framework we propose, we believe latter to be a better choice anyway. In fact, the quantile one contains all the necessary information whereas the mean one is a rough approximation. And, with all the available information, LASSO still does not include any near-mean values among the selected covariates.

The covariates selected by LASSO also provide additional interesting results. In fact, among the six mostly selected covariates, LASSO brought two TWI quantiles into the model. This is a hint that the common choice of BLR, a Generalized Linear Model, may not be the right one in this case. Other models, able to accomodate non-linearities, may produce

better results. Genaralized Additive Models for instance, could be a natural extension to the present framework. This consideration is not trivial because the traditional use of BLR implies that covariates are approximated or assumed to behave linearly. However, there is no guarantee that this approach would pay off. Performance-wise, BLR results are more than satisfying. Nevertheless, a more flexible approach may lead to a better interpretation of within-slope-unit dynamics and their effect on slope stability.

Another relevant consideration should be made regarding the generation of the shallow landslide inventory. The two available options currently consist of manual and semi-automated mapping. The former is expert-based, non-objective and time-consuming. The second one is consistent and fast. However, semi-automated approaches (here we chose OBIA) still produce a significant amount of False Positives and still merge different shallow landslides sources into a single polygon. In particular, the second disadvantage represents a significant issue for landslide susceptibility studies where having different source areas is vital to train the predictive model. In this work, we tried to combine the strengths of the two approaches. We quickly produced a semi-automated polygonal inventory, as our baseline for shallow landslides information. Subsequently, we refined the inventory by filtering out misclassifications occurring on natural rock outcrops. And, we manually digitized source points for those activation lobes that OBIA mistakenly merged. Nevertheless, considering the extension of the investigated area (181 km^2) and the large number of detected landslides (1939 polygons), OBIA considerably sped up the time required to produce the landslides inventory. This is a particularly relevant information in geoscience for semi-automatic mapping is a powerful tool but not yet ready to fully support landslide susceptibility models in an automated pipeline.

Future extensions to the workflow we propose could include different landslide types (e.g., shallow and deep-seated) to compare the covariates' effects and interpret their inherited differences due to different failure mechanisms. Nevertheless, in cases of deep-seated phenomena or rock avalanches and rock falls, automatic mapping techniques like OBIA may not equally

perform across different landslide classes and other procedures might be required to produce multi-class landslides inventories of comparable quality and completeness. In fact, current researches has mainly lead to semi-automated mapping applications for large landslides valid for single bodies (e.g., Niethammer *et al.*, 2012) rather than over multiple slopes.

In conclusion, the approach we tested can be extended to all those areas where landslides widely trigger over space. For instance, strong earthquakes typically produce thousands or tens of thousands of landslides, making the mapping procedure quite slow. OBIA could initially extract the landslide signature. This information could be integrated with ground motion data to support decisions in near real-time (e.g., Tanya and Lombardo, 2019). In fact, during seismic swarms, strong aftershocks can cause additional damage to the one due to the main shock. Knowing in near real-time the susceptible areas to new landslides, in between the main and after shocks, could be extremely useful to better manage the emergency phases.

A LASSO vs Stepwise Selection

Stepwise and LASSO techniques are motivated by the issue of having many potential predictors, but not enough data to estimate their coefficients. Both methods can be used to find a *best* model or to limit the number of predictors. In that line, stepwise proposes to include and/or exclude predictors according to their *statistical significance*, whereas LASSO uses a tuning parameter to penalize the number of parameters in the model, adding a sense of parsimony to the process. The main problems with stepwise methods have been identified and summarized in Harrell Jr (2015). Specifically, the F statistics do not have the claimed distribution, p-values might be too small due do multiple comparison issues, and standard errors of the parameter estimates are too small. Moreover, the method may not identify sets of variables that fit well, even when such sets exist (Miller, 2002). With LASSO, finding the optimal tuning parameter might be computationally costly, but it encourages shrinking of coefficients to 0, which is desirable in our setting, although it might not make sense to all types of data. Note that in our case, LASSO converges to a solution every time, while the stepwise method fails to converge more than 70% of the time (see the y axis of the right panel in Figure 5).

References

Alvioli, M., Marchesini, I. and Guzzetti, F. (2018) Nation-wide, general-purpose delineation of geomorphological slope units in Italy. Technical report, PeerJ Preprints.

Alvioli, M., Marchesini, I., Reichenbach, P., Rossi, M., Ardizzone, F., Fiorucci, F. and Guzzetti, F. (2016) Automatic delineation of geomorphological slope units with r. slopeunits v1. 0 and their optimization for landslide susceptibility modeling. *Geoscientific Model Development* **9**(11), 3975.

Arnone, E., Francipane, A., Scarbaci, A., Puglisi, C. and Noto, L. (2016) Effect of raster resolution and polygon-conversion algorithm on landslide susceptibility mapping. *Environmental Modelling & Software* **84**, 467–481.

Baatz, M., Schäpe, A., Strobl, J., Blaschke, T. and Griesebner, G. (2000) Multiresolution segmentation-an optimization approach for high quality multi-scale image segmentation. angewandte geographische informationsverarbeitung, 12, 12–23. retrieved from internal-pdf. *xn–baatz_schpe_2000-3891068462-jkc/Baatz_Sch* .

Beven, K. and Kirkby, M. J. (1979) A physically based, variable contributing area model of basin hydrology/Un modèle à base physique de zone d'appel variable de l'hydrologie du bassin versant. *Hydrological Sciences Journal* **24**(1), 43–69.

Boeckli, L., Brenning, A., Gruber, S. and Noetzli, J. (2012) Permafrost distribution in the European Alps: calculation and evaluation of an index map and summary statistics. *The Cryosphere* **6**(4), 807.

Böhner, J. and Selige, T. (2006) Spatial prediction of soil attributes using terrain analysis and climate regionalisation. *Gottinger Geographische Abhandlungen* **115**, 13–28.

Bosellini, A., Gianolla, P., Stefani, M. *et al.* (2003) Geology of the Dolomites. *Episodes* **26**(3), 181–185.

672 Bout, B., Lombardo, L., van Westen, C. J. and Jetten, V. G. (2018) Integration of two-phase
673 solid fluid equations in a catchment model for flashfloods, debris flows and shallow slope
674 failures. *Environmental modelling & software* **105**, 1–16.

675 Brenning, A. (2005) Spatial prediction models for landslide hazards: review, comparison and
676 evaluation. *Natural Hazards and Earth System Science* **5**(6), 853–862.

677 Budimir, M., Atkinson, P. and Lewis, H. (2015) A systematic review of landslide probability
678 mapping using logistic regression. *Landslides* **12**(3), 419–436.

679 Büttner, G. (2014) CORINE land cover and land cover change products. In *Land Use and*
680 *Land Cover Mapping in Europe*, pp. 55–74. Springer.

681 Cama, M., Conoscenti, C., Lombardo, L. and Rotigliano, E. (2016) Exploring relationships
682 between grid cell size and accuracy for debris-flow susceptibility models: a test in the
683 Giampilieri catchment (Sicily, Italy). *Environmental Earth Sciences* **75**(3), 1–21.

684 Cama, M., Lombardo, L., Conoscenti, C., Agnesi, V. and Rotigliano, E. (2015) Predicting
685 storm-triggered debris flow events: application to the 2009 Ionian Peloritan disaster (Sicily,
686 Italy). *Nat Hazards Earth Syst Sci* **15**(8), 1785–1806.

687 Carrara, A. (1988) Drainage and divide networks derived from high-fidelity digital terrain
688 models. In *Quantitative analysis of mineral and energy resources*, pp. 581–597. Springer.

689 Carrara, A., Cardinali, M., Detti, R., Guzzetti, F., Pasqui, V. and Reichenbach, P. (1991) Gis
690 techniques and statistical models in evaluating landslide hazard. *Earth surface processes*
691 *and landforms* **16**(5), 427–445.

692 Carrara, A., Crosta, G. and Frattini, P. (2008) Comparing models of debris-flow susceptibility
693 in the alpine environment. *Geomorphology* **94**(3-4), 353–378.

694 Casagli, N., Cigna, F., Bianchini, S., Hlbling, D., Freder, P., Righini, G., Conte, S. D., Friedl,
695 B., Schneiderbauer, S., Iasio, C., Vlcko, J., Greif, V., Proske, H., Granica, K., Falco, S.,

Lozzi, S., Mora, O., Arnaud, A., Novali, F. and Bianchi, M. (2016) Landslide mapping and monitoring by using radar and optical remote sensing: Examples from the EC-FP7 project SAFER. *Remote Sensing Applications: Society and Environment* **4**, 92 – 108.

Castro Camilo, D., Lombardo, L., Mai, P. M., Jie, D. and Huser, R. (2017) Handling high predictor dimensionality in slope-unit-based landslide susceptibility models through LASSO-penalized Generalized Linear Model. *Environmental Modelling and Software* **97**, 145–156.

Chen, X., Chen, H., You, Y. and Liu, J. (2015) Susceptibility assessment of debris flows using the analytic hierarchy process method- A case study in Subao river valley, China. *Journal of Rock Mechanics and Geotechnical Engineering* **7**(4), 404–410.

Copas, J. B. and Long, T. (1991) Estimating the Residual Variance in Orthogonal Regression with Variable Selection. *Journal of the Royal Statistical Society. Series D (The Statistician)* **40**(1), 51–59.

Costa, G., Feitosa, R., Fonseca, L., Oliveira, D., Ferreira, R. and Castejon, E. (2010) Knowledge-based interpretation of remote sensing data with the InterIMAGE system: major characteristics and recent developments. *Proceedings of the 3rd GEOBIA* .

Costa, J. E. (1984) Physical geomorphology of debris flows. In *Developments and applications of geomorphology*, pp. 268–317. Springer.

Derksen, S. and Keselman, H. J. (1992) Backward, forward and stepwise automated subset selection algorithms: Frequency of obtaining authentic and noise variables. *British Journal of Mathematical and Statistical Psychology* **45**(2), 265–282.

Dormann, C. F., Elith, J., Bacher, S., Buchmann, C., Carl, G., Carr, G., Marquz, J. R. G., Gruber, B., Lafourcade, B., Leito, P. J., Mnkemller, T., McClean, C., Osborne, P. E., Reineking, B., Schrder, B., Skidmore, A. K., Zurell, D. and Lautenbach, S. (2013) Collinearity: a review of methods to deal with it and a simulation study evaluating their performance. *Ecography* **36**(1), 27–46.

721 Eisank, C., Hölbling, D., Friedl, B., Chen, Y. and Chang, K. (2014) Expert knowledge for
722 object-based landslide mapping in Taiwan. *S East Eur J Earth Obs Geomat Spec Issue:*
723 *GEOBIA* pp. 347–350.

724 Erener, A. and Düzgün, H. (2012) Landslide susceptibility assessment: what are the effects
725 of mapping unit and mapping method? *Environmental Earth Sciences* **66**(3), 859–877.

726 Fan, X., Juang, C. H., Wasowski, J., Huang, R., Xu, Q., Scaringi, G., van Westen, C. J. and
727 Havenith, H.-B. (2018) What we have learned from the 2008 Wenchuan Earthquake and
728 its aftermath: A decade of research and challenges. *Engineering geology* **241**, 25–32.

729 Finke, P. and Montanarella, L. (2001) Basic Principals of the Manual of Procedures (Version
730 1.1) for the Georeferenced Soil Database. *Options Méditerranéennes: Série B. Etudes et*
731 *Recherches* (34), 49–65.

732 Forman, R. T. and Godron, M. (1986) Landscape ecology John Wiley & Sons. *New York* **4**,
733 22–28.

734 Frattini, P., Crosta, G. and Carrara, A. (2010) Techniques for evaluating the performance
735 of landslide susceptibility models. *Engineering Geology* **111**(1), 62–72.

736 Ghinoi, A. and Chung, C.-J. (2005) STARTER: a statistical GIS-based model for the predic-
737 tion of snow avalanche susceptibility using terrain featuresapplication to Alta Val Badia,
738 Italian Dolomites. *Geomorphology* **66**(1-4), 305–325.

739 Guzzetti, F., Galli, M., Reichenbach, P., Ardizzone, F. and Cardinali, M. (2006) Landslide
740 hazard assessment in the collazzone area, umbria, central italy. *Natural Hazards and Earth*
741 *System Science* **6**(1), 115–131.

742 Hansen, A. (1984) Landslide hazard analysis. *Slope instability. Wiley, New York* pp. 523–602.

743 Harrell Jr, F. E. (2015) *Regression modeling strategies: with applications to linear models,*
744 *logistic and ordinal regression, and survival analysis*. Springer.

745 Hay, G. J. and Castilla, G. (2008) Geographic Object-Based Image Analysis (GEOBIA): A
746 new name for a new discipline. In *Object-based image analysis*, pp. 75–89. Springer.

747 Heerdegen, R. G. and Beran, M. A. (1982) Quantifying source areas through land surface
748 curvature and shape. *Journal of Hydrology* **57**(3-4), 359–373.

749 Hölbling, D., Eisank, C., Albrecht, F., Vecchiotti, F., Friedl, B., Weinke, E. and Kociu,
750 A. (2017) Comparing Manual and Semi-Automated Landslide Mapping Based on Optical
751 Satellite Images from Different Sensors. *Geosciences* **7**(2), 37.

752 Hölbling, D., Füreder, P., Antolini, F., Cigna, F., Casagli, N. and Lang, S. (2012) A semi-
753 automated object-based approach for landslide detection validated by persistent scatterer
754 interferometry measures and landslide inventories. *Remote Sensing* **4**(5), 1310–1336.

755 Horton, A. J., Hales, T. C., Ouyang, C. and Fan, X. (2019) Identifying post-earthquake
756 debris flow hazard using massflow. *Engineering Geology* **258**, 105134.

757 Hosmer, D. W. and Lemeshow, S. (2000) *Applied Logistic Regression*. Second edition. New
758 York: Wiley.

759 Hu, X., Hu, K., Tang, J., You, Y. and Wu, C. (2019) Assessment of debris-flow potential
760 dangers in the Jiuzhaigou Valley following the August 8, 2017, Jiuzhaigou earthquake,
761 western China. *Engineering Geology* **256**, 57–66.

762 Hungr, O., Leroueil, S. and Picarelli, L. (2014) The Varnes classification of landslide types,
763 an update. *Landslides* **11**(2), 167–194.

764 Hutchinson, J. (1988) General report, morphological and geotechnical parameters of land-
765 slides in relation to geology and hydrogeology. In *Landslides, Proceedings of the Fifth*
766 *International Symposium on Landslides, 1988*.

767 Imaizumi, F., Sidle, R. C., Tsuchiya, S. and Ohsaka, O. (2006) Hydrogeomorphic processes
768 in a steep debris flow initiation zone. *Geophysical Research Letters* **33**(10).

769 Iverson, R. M., Reid, M. E. and LaHusen, R. G. (1997) Debris-flow mobilization from land-
770 slides. *Annual Review of Earth and Planetary Sciences* **25**(1), 85–138.

771 Ko, F. W. and Lo, F. L. (2018) From landslide susceptibility to landslide frequency: A
772 territory-wide study in Hong Kong. *Engineering geology* **242**, 12–22.

773 Lan, H., Zhou, C., Wang, L., Zhang, H. and Li, R. (2004) Landslide hazard spatial analysis
774 and prediction using GIS in the Xiaojiang watershed, Yunnan, China. *Engineering geology*
775 **76**(1-2), 109–128.

776 Lin, C.-H. and Lin, M.-L. (2015) Evolution of the large landslide induced by Typhoon
777 Morakot: a case study in the Butangbunasi River, southern Taiwan using the discrete
778 element method. *Engineering geology* **197**, 172–187.

779 Lin, C.-H., Lin, M.-L., Peng, H.-R. and Lin, H.-H. (2018) Framework for susceptibility anal-
780 ysis of layered rock slopes considering the dimensions of the mapping units and geological
781 data resolution at various map scales. *Engineering geology* **246**, 310–325.

782 Lombardo, L., Bakka, H., Tanyas, H., van Westen, C., Mai, P. M. and Huser, R. (2019) Geo-
783 statistical modeling to capture seismic-shaking patterns from earthquake-induced land-
784 slides. *Journal of Geophysical Research: Earth Surface* **124**, In press.

785 Lombardo, L., Cama, M., Conoscenti, C., Märker, M. and Rotigliano, E. (2015) Binary
786 logistic regression versus stochastic gradient boosted decision trees in assessing landslide
787 susceptibility for multiple-occurring landslide events: application to the 2009 storm event
788 in Messina (Sicily, southern Italy). *Natural Hazards* **79**(3), 1621–1648.

789 Lombardo, L., Cama, M., Maerker, M. and Rotigliano, E. (2014) A test of transferability for
790 landslides susceptibility models under extreme climatic events: application to the Messina
791 2009 disaster. *Natural hazards* **74**(3), 1951–1989.

792 Lombardo, L., Fubelli, G., Amato, G. and Bonasera, M. (2016) Presence-only approach to
793 assess landslide triggering-thickness susceptibility: a test for the Mili catchment (north-
794 eastern Sicily, Italy). *Natural hazards* **84**(1), 565–588.

795 Lombardo, L. and Mai, P. (2018) Presenting logistic regression-based landslide susceptibility
796 results. *Engineering Geology* **244**, 14–24.

797 Lombardo, L., Opitz, T. and Huser, R. (2018a) Point process-based modeling of multiple
798 debris flow landslides using INLA: an application to the 2009 Messina disaster. *Stochastic*
799 *Environmental Research and Risk Assessment* **32**(7), 2179–2198.

800 Lombardo, L., Saia, S., Schillaci, C., Mai, P. M. and Huser, R. (2018b) Modeling soil or-
801 ganic carbon with Quantile Regression: Dissecting predictors' effects on carbon stocks.
802 *Geoderma* **318**, 148–159.

803 Marchetti, M., Ghinoi, A. and Soldati, M. (2017) The Dolomite Landscape of the Alta Badia
804 (Northeastern Alps): A Remarkable Record of Geological and Geomorphological History.
805 In *Landscapes and Landforms of Italy*, pp. 123–134. Springer.

806 Martha, T. R., Kerle, N., Jetten, V., van Westen, C. J. and Kumar, K. V. (2010) Char-
807 acterising spectral, spatial and morphometric properties of landslides for semi-automatic
808 detection using object-oriented methods. *Geomorphology* **116**(1-2), 24–36.

809 Mathew, J., Jha, V. and Rawat, G. (2009) Landslide susceptibility zonation mapping and
810 its validation in part of Garhwal Lesser Himalaya, India, using binary logistic regression
811 analysis and receiver operating characteristic curve method. *Landslides* **6**(1), 17–26.

812 Miller, A. (2002) *Subset selection in regression*. Chapman and Hall/CRC.

813 Moore, I. D., Grayson, R. and Ladson, A. (1991) Digital terrain modelling: a review of
814 hydrological, geomorphological, and biological applications. *Hydrological processes* **5**(1),
815 3–30.

816 Nachtergaele, F. (2010) The classification of Leptosols in the World Reference Base for Soil
817 Resources. In *19th World Congress of Soil Science, Soil Solutions for a Changing World*,
818 pp. 1–6.

819 Niethammer, U., James, M., Rothmund, S., Travelletti, J. and Joswig, M. (2012) UAV-based
820 remote sensing of the Super-Sauze landslide: Evaluation and results. *Engineering Geology*
821 **128**, 2–11.

822 Piacentini, D., Troiani, F., Soldati, M., Notarnicola, C., Savelli, D., Schneiderbauer, S. and
823 Strada, C. (2012) Statistical analysis for assessing shallow-landslide susceptibility in South
824 Tyrol (south-eastern Alps, Italy). *Geomorphology* **151**, 196–206.

825 Pourghasemi, H. R. and Rossi, M. (2016) Landslide susceptibility modeling in a landslide
826 prone area in Mazandarn Province, north of Iran: a comparison between GLM, GAM,
827 MARS, and M-AHP methods. *Theoretical and Applied Climatology* pp. 1–25.

828 Raja, N. B., Çiçek, I., Türkoğlu, N., Aydin, O. and Kawasaki, A. (2017) Landslide suscep-
829 tibility mapping of the Sera River Basin using logistic regression model. *Natural Hazards*
830 **85**(3), 1323–1346.

831 Rau, J., Jhan, J., Lo, C. and Lin, Y. (2011) Landslide mapping using imagery acquired by
832 a fixed-wing UAV. *Int. Arch. Photogramm. Remote Sens. Spat. Inf. Sci* **38**, 1–C22.

833 Reichenbach, P., Rossi, M., Malamud, B. D., Mihir, M. and Guzzetti, F. (2018) A review of
834 statistically-based landslide susceptibility models. *Earth-science reviews* **180**, 60–91.

835 Riley, S. J., DeGloria, S. and Elliot, R. (1999) Index that quantifies topographic heterogene-
836 ity. *Intermountain Journal of sciences* **5**(1-4), 23–27.

837 Rossi, M., Guzzetti, F., Reichenbach, P., Mondini, A. C. and Peruccacci, S. (2010) Optimal
838 landslide susceptibility zonation based on multiple forecasts. *Geomorphology* **114**(3), 129–
839 142.

840 Rouse Jr, J., Haas, R., Schell, J. and Deering, D. (1974) Monitoring vegetation systems in
841 the Great Plains with ERTS .

842 Schillaci, C., Acutis, M., Vesely, F. and Saia, S. (2019) A simple pipeline for the assessment
843 of legacy soil datasets: An example and test with soil organic carbon from a highly variable
844 area. *Catena* **175**, 110–122.

845 Schlögel, R., Marchesini, I., Alvioli, M., Reichenbach, P., Rossi, M. and Malet, J.-P. (2018)
846 Optimizing landslide susceptibility zonation: Effects of DEM spatial resolution and slope
847 unit delineation on logistic regression models. *Geomorphology* **301**, 10–20.

848 Schlögel, R., Thiebes, B., Mulas, M., Cuozzo, G., Notarnicola, C., Schneiderbauer, S., Crespi,
849 M., Mazzoni, A., Mair, V. and Corsini, A. (2017) Multi-temporal X-Band radar inter-
850 ferometry using corner reflectors: Application and validation at the Corvara Landslide
851 (Dolomites, Italy). *Remote Sensing* **9**(7), 739.

852 Soldati, M., Corsini, A. and Pasuto, A. (2004) Landslides and climate change in the Italian
853 Dolomites since the Late glacial. *Catena* **55**(2), 141–161.

854 Süzen, M. L. and Kaya, B. Ş. (2012) Evaluation of environmental parameters in logistic
855 regression models for landslide susceptibility mapping. *International Journal of Digital*
856 *Earth* **5**(4), 338–355.

857 Tacchia, D., Masella, G., Pannnuti, V. and Vitale, V. (2005) La nuova Carta Geologica
858 dItalia scala 1: 1.000.000. *Geologica d'Italia alla scala* **1**(1.000), 000.

859 Tanya, H. and Lombardo, L. (2019) Variation in landslide-affected area under the control of
860 ground motion and topography. *Engineering Geology* **260**, 105229.

861 Tian, Y., Xiao, C. and Wu, L. (2010) Slope unit-based landslide susceptibility zonation. In
862 *Geoinformatics, 2010 18th International Conference on*, pp. 1–5.

Tibshirani, R. (1996) Regression shrinkage and selection via the LASSO. *Journal of the Royal Statistical Society. Series B (Methodological)* pp. 267–288.

Tiede, D., Lang, S., Albrecht, F. and Hölbling, D. (2010) Object-based class modeling for cadastre-constrained delineation of geo-objects. *Photogrammetric Engineering & Remote Sensing* **76**(2), 193–202.

Tiranti, D., Crema, S., Cavalli, M. and Deangeli, C. (2018) An integrated study to evaluate debris flow hazard in alpine environment. *Frontiers in Earth Science* **6**, 60.

Trigila, A., Iadanza, C. and Guerrieri, L. (2007) The IFFI project (Italian landslide inventory): Methodology and results. *Guidelines for Mapping Areas at Risk of Landslides in Europe* **23**, 15.

Đurić, U., Marjanović, M., Radić, Z. and Abolmasov, B. (2019) Machine learning based landslide assessment of the Belgrade metropolitan area: Pixel resolution effects and a cross-scaling concept. *Engineering Geology* **256**, 23–38.

Van Den Eeckhaut, M., Reichenbach, P., Guzzetti, F., Rossi, M. and Poesen, J. (2009) Combined landslide inventory and susceptibility assessment based on different mapping units: an example from the Flemish Ardennes, Belgium. *Natural Hazards and Earth System Sciences* **9**(2), 507–521.

Van Westen, C. J., Castellanos, E. and Kuriakose, S. L. (2008) Spatial data for landslide susceptibility, hazard, and vulnerability assessment: An overview. *Engineering geology* **102**(3-4), 112–131.

Vandelli, V., Ghinoi, A., Marchetti, M. and Soldati, M. (2019) Discovery and dating of Pre-LGM deposits in a high catchment of the Dolomites (Italy): New insights on climate-related geomorphological processes during the Late Pleistocene. *Geomorphology* .

886 Working Group WRB, I. (2014) World Reference Base for Soil Resources 2014, International
887 Soil Classification System for Naming Soils and Creating Legends for Soil Maps, World
888 Soil Resources Reports No. 106 .

889 Yesilnacar, E. and Topal, T. (2005) Landslide susceptibility mapping: a comparison of lo-
890 gistic regression and neural networks methods in a medium scale study, Hendek region
891 (Turkey). *Engineering Geology* **79**(3-4), 251–266.

892 Zevenbergen, L. W. and Thorne, C. R. (1987) Quantitative analysis of land surface topog-
893 raphy. *Earth surface processes and landforms* **12**(1), 47–56.

894 Zhou, S., Fang, L. and Liu, B. (2015) Slope unit-based distribution analysis of landslides
895 triggered by the April 20, 2013, Ms 7.0 Lushan earthquake. *Arabian Journal of Geosciences*
896 **8**(10), 7855–7868.

897 Zou, H. and Hastie, T. (2005) Regularization and variable selection via the elastic net.
898 *Journal of the Royal Statistical Society: Series B (Statistical Methodology)* **67**(2), 301–
899 320.

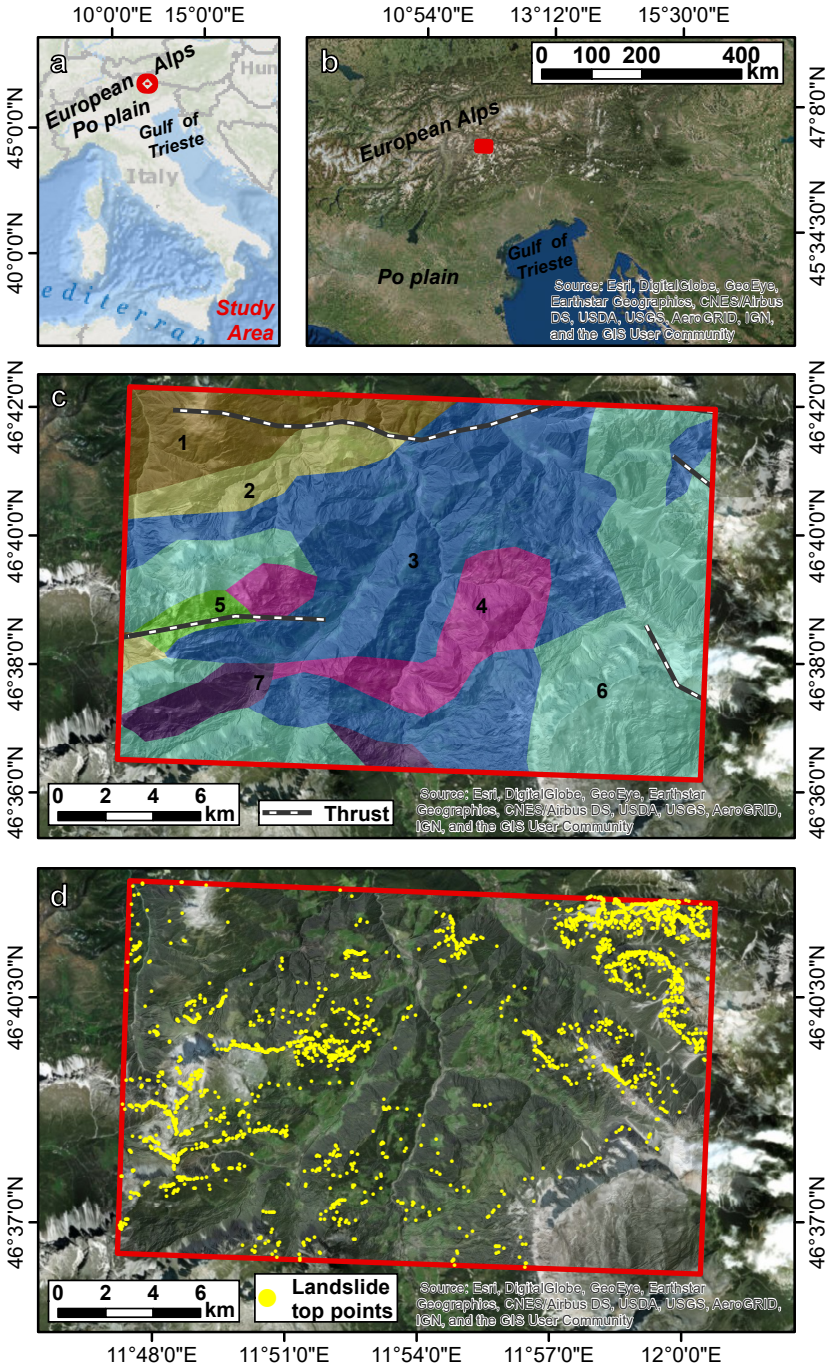

Figure 1: *a*) and *b*) national and regional geographic contexts. c) shows the outcropping lithologies: 1 = South-alpine metamorphic complex; 2 = Gardena Sandstone Fm; 3 = Werfen Fm and San Cassiano Fm; 4 = Wengen Fm; 5 = Sciliar Fm; 6 = Dolomia Principale Fm and Calcari Grigi Fm; 7 = Glacial deposits. *d*) Landslides source locations approximated as the highest point along the landslide perimeter.

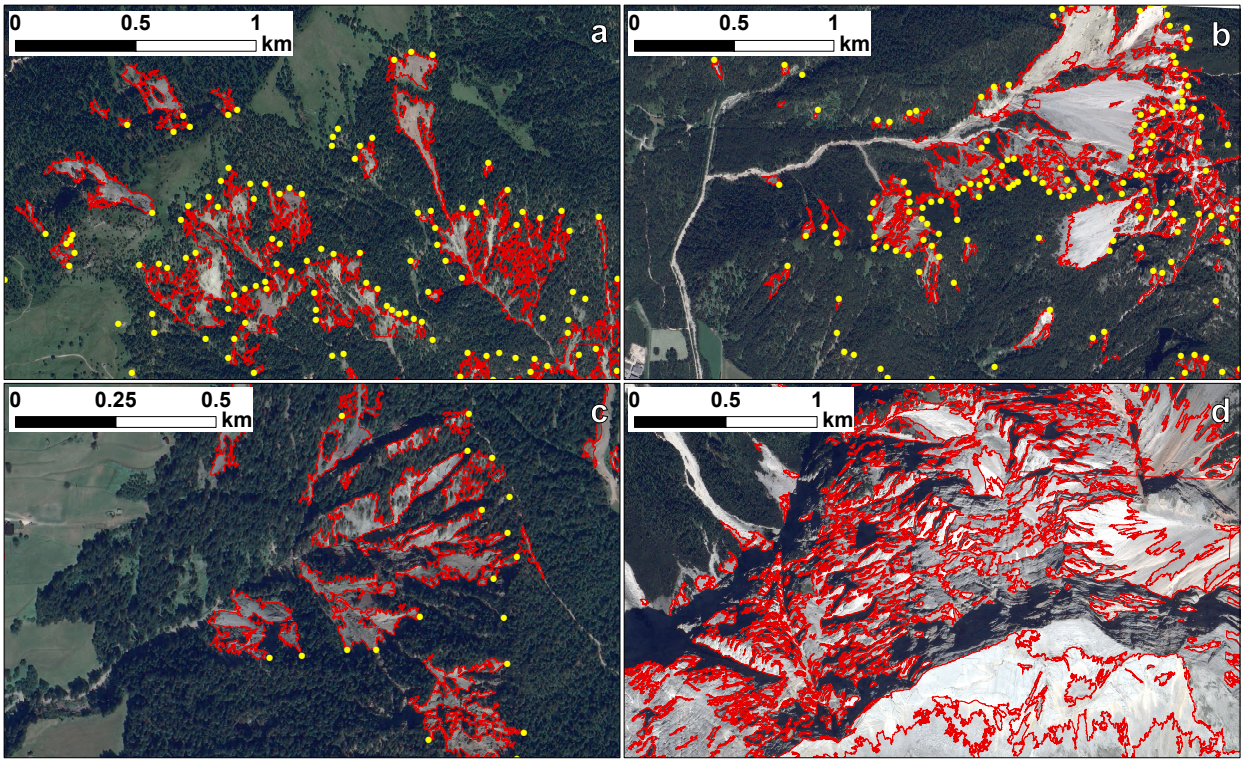

Figure 2: (*a, b, c*) Examples where OBIA correctly maps landslides (*d*) Type 1 errors made by OBIA: false positives are mapped where dolomites naturally outcrop.

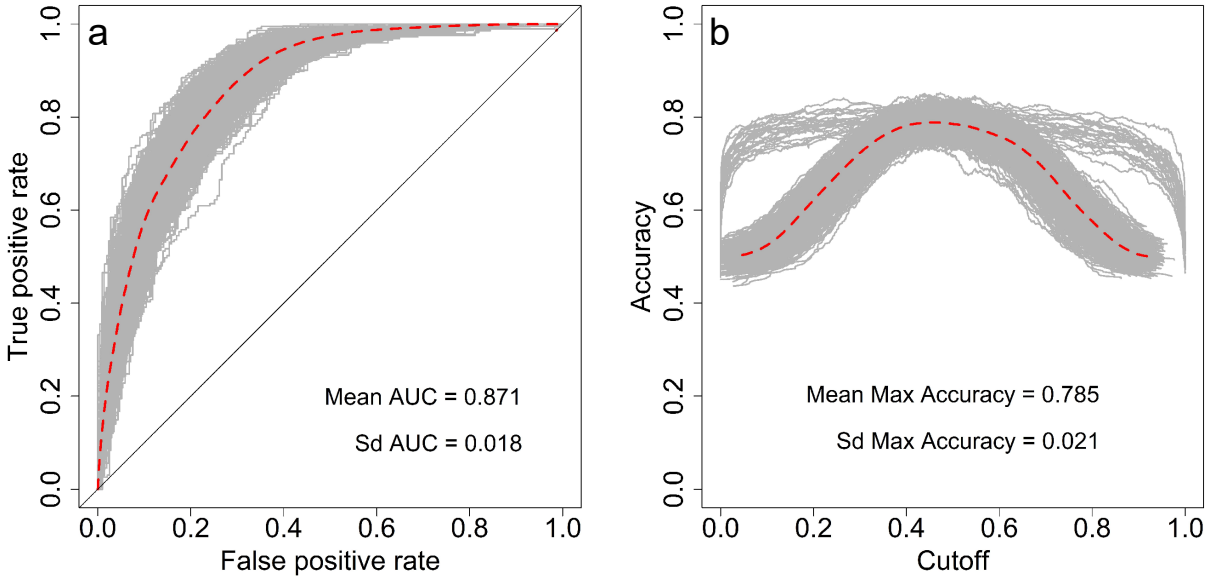

Figure 3: (*a*) Cross-validation ROC curves obtained for each replicate, shown in grey, and their mean curve, shown in red. (*b*) Cross-validation Accuracy curves obtained for each replicate, shown in grey, and their mean curve, shown in red.

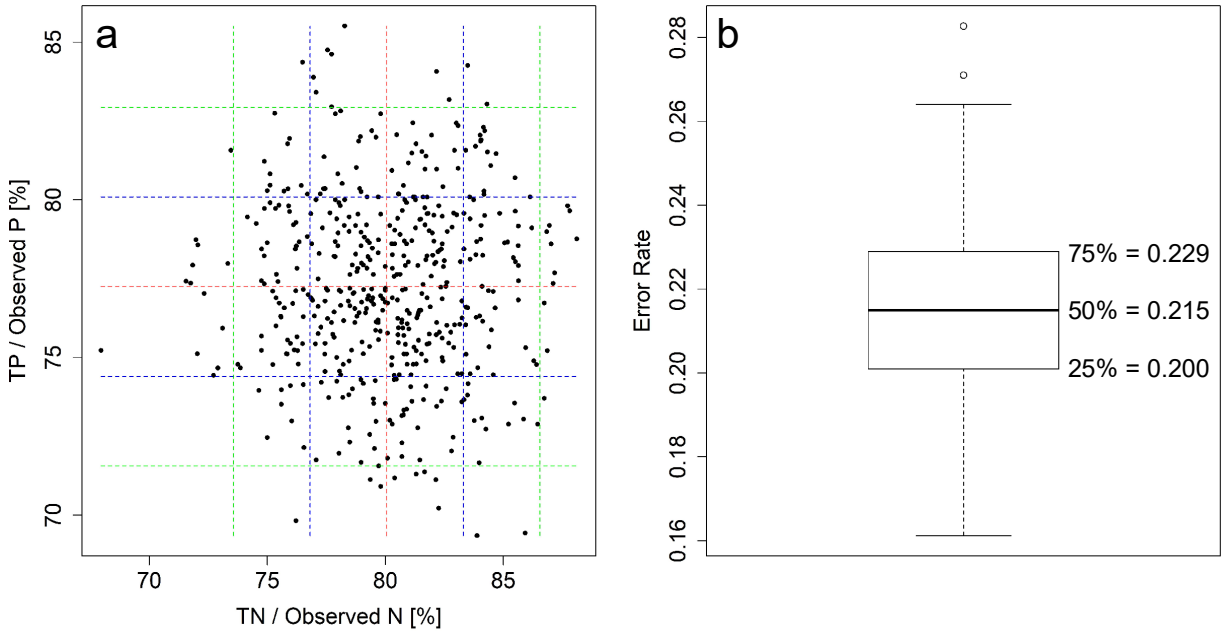

Figure 4: (a) Confusion plot showing the ratios between True prediction and total sample, for Negative (abscissa) and Positive (ordinate) cases and for each of the 500 cross-validation replicates. Red lines represent the mean, blue lines correspond to one standard deviation and green lines are expressed as two times the standard deviation. (b) Error rate distribution across replicates.

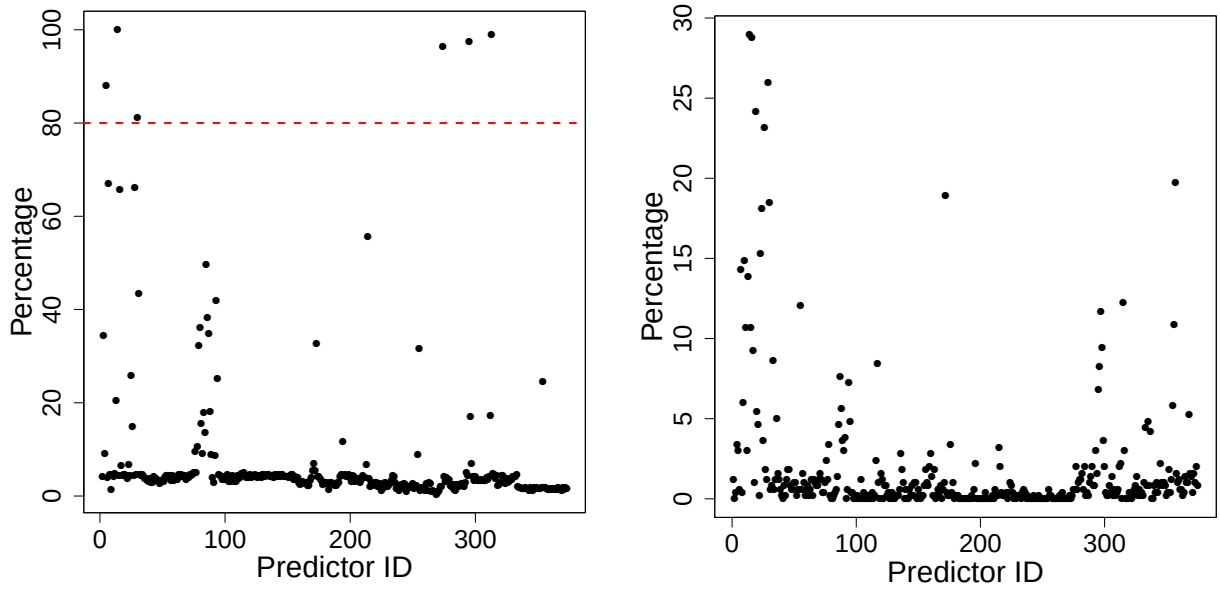

Figure 5: Percentage of LASSO (left panel) and Stepwise (right panel) selection among 500 replicates. For the right panel, the upper limit of the y-axis is 30% because Stepwise cannot converge to a solution for 356 replicates out of 500. In other words, Stepwise failed 71.2% of the times.

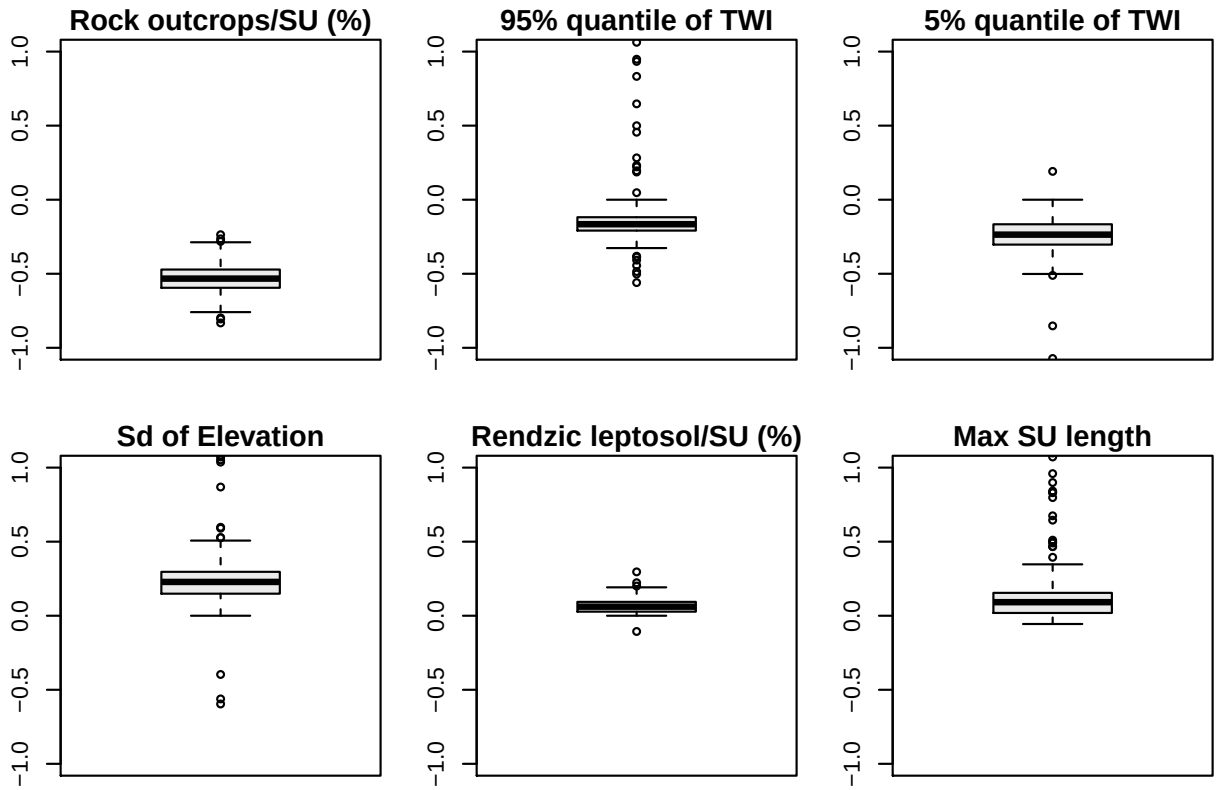

Figure 6: Boxplot of the regression coefficients' distribution for the six most selected covariates.

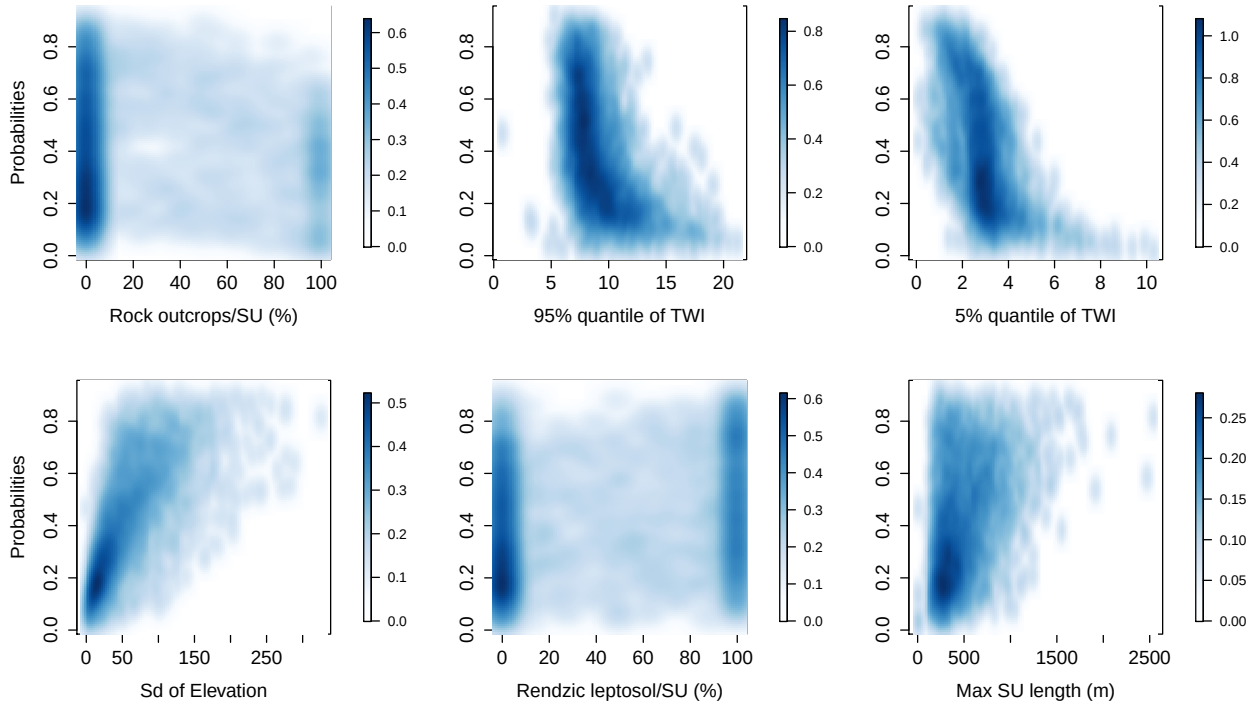

Figure 7: Response plot between the mean susceptibility computed across replicates and the original covariate domain.

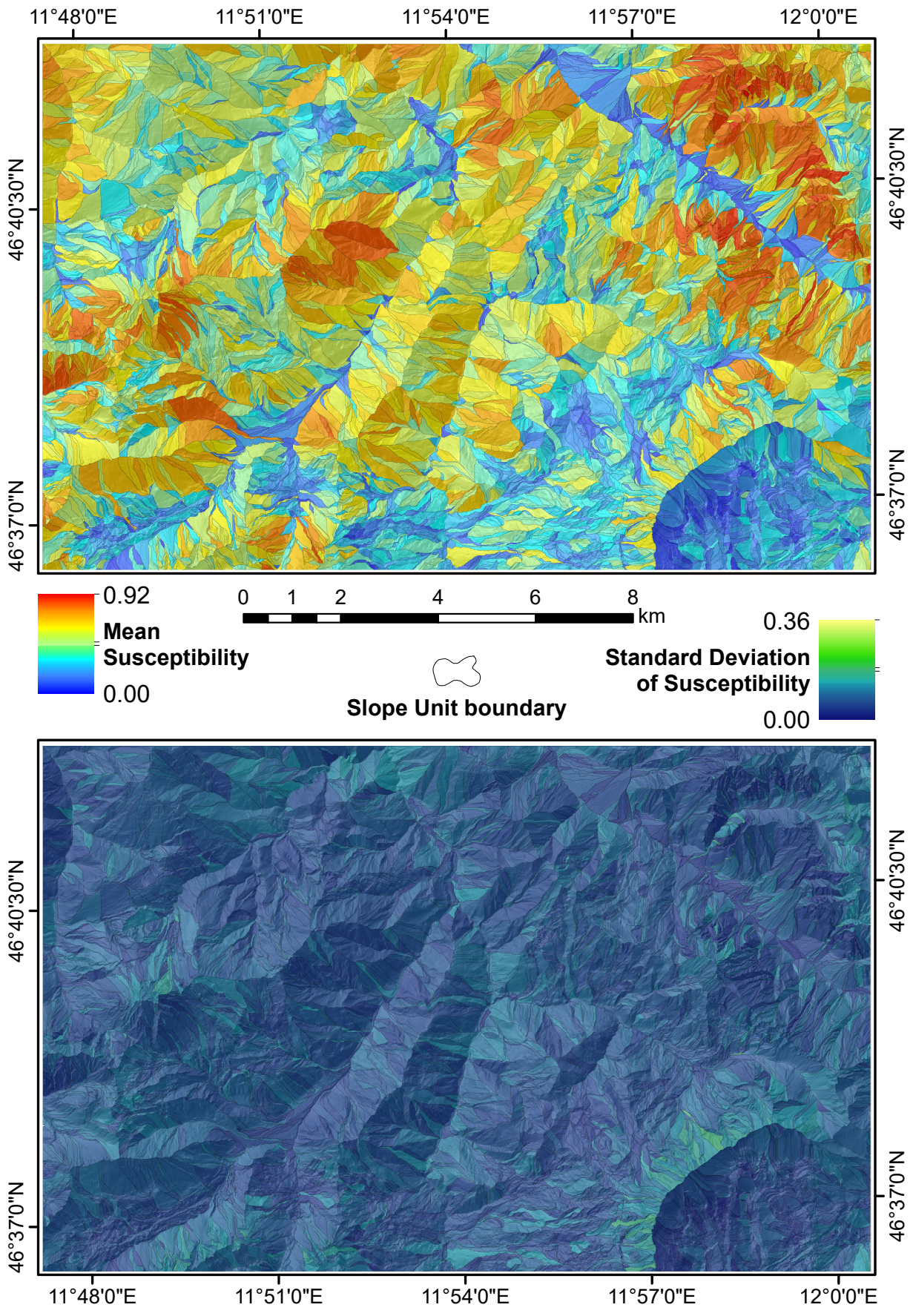

Figure 8: Mean susceptibility and its associated standard deviation across the 500 replicates.

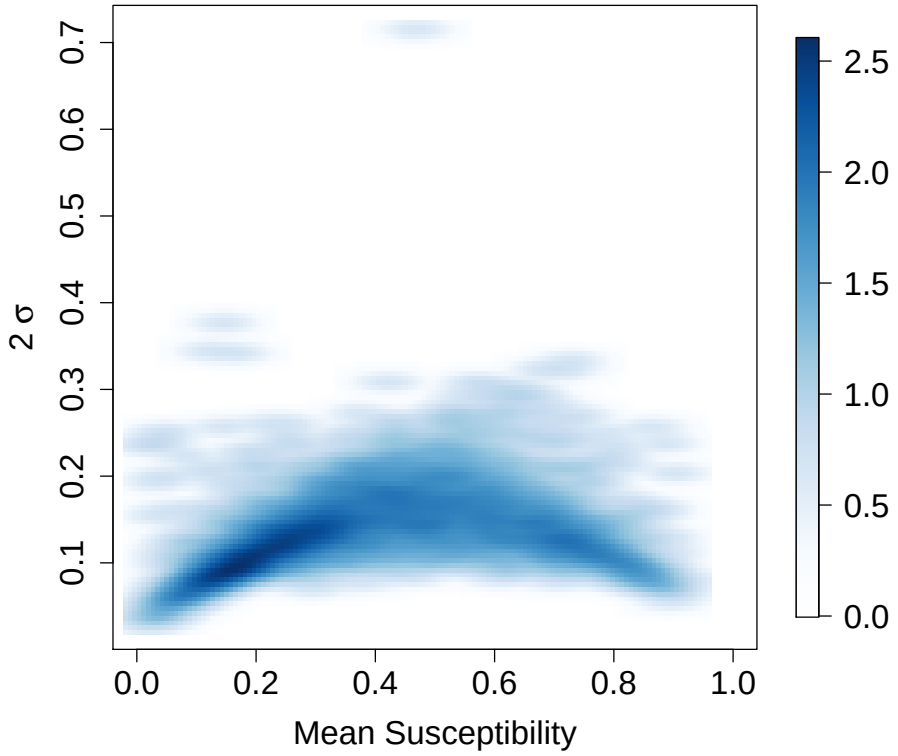

Figure 9: Mean susceptibility plotted against twice its standard deviation across the 500 replicates.